

On the relevance of molecular diffusion for travel time distributions inferred from different water isotopes

Erwin Zehe¹, Laurent Pfister^{2,3}, Dan Elhanati⁴, Brian Berkowitz⁴

1. Institute of Water and Environment, Karlsruhe Institute of Technology (KIT), 76131 Karlsruhe, Germany
2. Luxembourg Institute of Science and Technology, Environmental Sensing & Modelling Unit, 41 rue du Brill, L-4422 Belvaux, Luxembourg
3. University of Luxembourg, Faculty of Science, Technology and Medicine, 2 place de l'Université, L-4365 Esch-sur-Alzette, Luxembourg
4. Department of Earth and Planetary Sciences, Weizmann Institute of Science, Rehovot 7610001, Israel

Correspondence to: Erwin Zehe (Erwin.Zehe@kit.edu)

Abstract: Water isotopes are a tool of choice for assessing travel time distributions of water ~~and chemical species~~ in soils, aquifers and rivers. However, the question of whether different water isotopes tag the same travel time distributions of the water molecule, or whether the inferred travel time distribution is specific to the chosen water isotope, remains under debate. Here we conjecture that the latter is correct. We state that (a) travel time distributions of water and any tracer reflect the spectrum of fluid velocities and diffusive/dispersive mixing between the flow lines connecting the system in- and outlet, and (b) the ~~self~~ diffusion coefficients of deuterium, tritium and ¹⁸O differ by as much as 10%. Using particle tracking simulations, we show that these differences do indeed affect the variance of the travel time distribution – as one would expect for well-mixed advective-dispersive transport. Moreover, our simulations suggest that in the case of imperfect mixing, also the average travel time becomes sensitive to the differences in ~~self~~ diffusion coefficients. We find that when advective trapping occurs in low conductive zones, an isotope with a smaller diffusion coefficient remains there for longer times compared to a substance exhibiting faster diffusion. This implies that for imperfectly mixed transport, average transit times ultimately increase with a decreasing ~~self~~ diffusion coefficient: deuterium has the longest average travel time, followed by tritium, followed by ¹⁸O. Depending on the type of simulated system, we find differences in average travel times ranging from 10 days to more than 2 years. As these differences are in relative terms ~~in most cases usually~~ of order 5-10%, one ~~could be tempted to might~~ erroneously explain them as measurement errors. Our findings suggest instead that these ~~relative~~ differences are physics based ~~and may reach up to relative differences of 30% for strongly heterogeneous systems-~~. ~~These differences~~ persisting and even growing with increasing space and time scales, rather than being averaged out. We thus conclude that travel time distributions inferred from O-H isotopes of the water molecule are conditioned by the chosen water isotope.

1 INTRODUCTION

Travel or transit time distributions play a key role in contaminant leaching from the partially saturated zone into groundwater (Sternagel et al., 2021; Klaus et al., 2013; Klaus et al., 2014) and stream flow chemistry in general (Kirchner et al., 2000). As early as 1982, Simmons (1982) and Jury (1982) introduced the concept of travel time and travel distance distributions into soil physics, to acknowledge that field observations of solute transport were frequently inconsistent with predictions of the advection-dispersion model. When injecting a tracer pulse into the soil,

46 the normalized concentration as function of depth characterizes the distribution of travel
47 distances at a fixed time, while the time series of the normalized concentration observed at a
48 constant depth yields the distribution of times the molecules need to travel to this depth (TTD).
49 Recalling the theory of linear systems, Simmons (1982) and Jury (1982) advocated the TTD,
50 also often referred to as solute breakthrough curve (BTC), as the transfer function for simulating
51 solute breakthrough to a given depth. **In line with this approach, Barnes and Bornel (1996)**

52 **applied unit hydrograph techniques to predict solute transport in catchments.**

hat formatiert: Hervorheben

hat formatiert: Hervorheben

hat formatiert: Hervorheben

53
54 The charm of this approach is that by using alternative transfer functions, one can step beyond
55 the limitations of advective-dispersive transport. The latter is also called Fickian transport and
56 reflects the case of perfect mixing, wherein chemical species visit the entire domain and thus
57 experience the entire spectrum of fluid velocities “many” times. In this case, the central limit
58 theorem applies, and normally distributed transport distances emerge and the variance in travel
59 distances grows linearly with time (Roth and Hammel, 1996). Simmons et al. (1982) showed
60 that a stochastic convective transfer function is well suited to simulate solute transport in the
61 yet imperfectly mixed near field, where the variance in travel distance grows with the squared
62 transport time. The general drawback here is that transfer function approaches require linearity
63 and thus a time invariant velocity field. However, water flow velocities do change nonlinearly
64 with soil water content, which means that TTD are conditional to (changing) soil water contents
65 and rainfall forcings. This explains notably why transfer function approaches are (despite their
66 mathematical appeal) of low practical relevance to predict solute leaching in soils.

67
68 **Naturally Strikingly, the concept of travel time distributions was used even earlier in**
69 **groundwater and catchment systems as reported by Erikson (1958) and Bolin and Rhode (1973).**

hat formatiert: Hervorheben

hat formatiert: Hervorheben

hat formatiert: Hervorheben

70 **Furthermore,** Berkowitz and Scher (1995) introduced the continuous time domain random walk
71 to simulate Fickian and non-Fickian transport of chemical species, which essentially uses
72 transfer functions characterizing travel time distributions of solutes inferred from observed
73 BTCs; see Berkowitz et al. (2006) for a detailed introduction. ~~A closer look reveals that~~
74 **Naturally,** travel or transit time distributions can also be defined for entire river basins
75 (McGlynn et al., 2002; McGlynn et al., 2003; Weiler et al., 2003; Hrachowitz et al., 2009;
76 Hrachowitz et al., 2016; Benettin et al., 2015; Benettin et al., 2018; Rodriguez et al., 2018;
77 Rodriguez et al., 2021), because catchments or watersheds drain the collected precipitation to
78 their stream outlet or release it via evapotranspiration. The defined “inlet” for rainfall and

79 tracers is hence the catchment surface/soil surface, while the defined outlet is either the riparian
80 zone when focusing on transit times of streamflow or the soil-vegetation system to infer transit
81 times of evaporation and transpiration. As flow velocities in the stream are several orders of
82 magnitude larger relative to those prevailing in the subsurface domain, tracer observations at
83 the catchment outlet yield a very good (lumped) approximation of the transit time distribution
84 of water and chemical species through the catchment system into the stream.

85
86 Early attempts to predict stream flow chemistry and related transit times relied also on transfer
87 functions (Barnes and Bonell, 1996; McGuire and McDonnell, 2006) and naturally faced the
88 same problems of state-dependent and seasonally varying travel time distributions. To
89 overcome this problem, Hrachowitz et al. (2013) proposed using mixing coefficients, while
90 Harmann et al. (2015) and Rinaldo et al. (2015) Klaus et al., 2015; Rodriguez et al., 2018).
91 Alternative approaches rely introduced the concept on of age ranked storage in combination
92 with StoreAgeSelection (SAS) functions for, e.g., stream flow to infer inferring the respective
93 travel time distributions of stream flow (Harmann et al. 2015; Rinaldo et al., 2015). This
94 requires the numerical solution of the Master Equation, i.e., the catchment water balance for
95 each time and each age (Rodriguez and Klaus, 2019) alongside an appropriate selection of the
96 functional form of SAS-function(s), e.g., as a gamma or beta distribution (Hrachowitz et al.,
97 2010; Klaus et al., 2015; Rodriguez and Klaus, 2019; van der Velde et al., 2012) and their
98 weights. Recent work reveals that this approach is even suited to capture fingerprints of
99 preferential flow in the partially saturated zone (Türk et al, 2025). A closer look reveals that the
100 use of mixing coefficients is functionally similar to the SAS approach using piece-wise linear
101 age sampling distributions, as shown by Hrachowitz et al. (2016).

102
103 Regardless of whether one favours the transfer function or the SAS approach Any attempt to
104 infer travel time distributions requires, essentially, the use of tracers; clearly -water isotopes
105 play a key role here as they s are in both cases used as a provide a time-continuous source of
106 information for this purpose transit time distributions at the pedon (Sprenger et al. 2016) and
107 the catchment scales (McGlynn et al., 2002; McGlynn and Seibert, 2003; Weiler et al., 2003;
108 Klaus et al., 2013; Sprenger et al., 2016). Yet to date, a controversial debate prevails as to
109 whether different water isotopes yield information on the same travel time distribution.
110 Rodriguez et al. (2021) found different median travel times of deuterium (1.77 y) and tritium
111 (2.19 y) in the 42 ha large Weierbach catchment in Luxembourg using an SAS approach

hat formatiert: Hervorheben

hat formatiert: Hervorheben

hat formatiert: Englisch (Vereinigte Staaten), Hervorheben

hat formatiert: Hervorheben

hat formatiert: Englisch (Vereinigte Staaten), Hervorheben

hat formatiert: Englisch (Vereinigte Staaten), Hervorheben

hat formatiert: Hervorheben

hat formatiert: Hervorheben

hat formatiert: Hervorheben

hat formatiert: Hervorheben

hat formatiert: Hervorheben

hat formatiert: Hervorheben

hat formatiert: Hervorheben

hat formatiert: Hervorheben

112 combining three different age distribution functions. However, the authors considered these
113 differences as unphysical, because they refer to two times “the same water molecule” and
114 explained these differences by mere measurement uncertainty. However, Stewart et al. (2010,
115 2021) report that average travel times inferred from ^{18}O and tritium might differ more than one
116 year and argued that these differences are significant and physics based. More recent work of
117 Wang et al. (2023) reported that the water ages and transit time distributions inferred from ^{18}O
118 and ^3H using the SAS approach were largely consistent, while related differences appeared
119 substantial; when using a convolution model approach. Obviously, comparative studies must
120 be very precise about their underlying methods for inferring travel times, to ensure that they are
121 comparing the same quantities.

122
123 Here we conjecture that travel time distributions are indeed specific to the chosen water isotope.
124 More specifically, we argue that (a) TTDs reflect the spectra of fluid velocities along the
125 flowlines of variable lengths *as well as* diffusive and/or dispersive mixing among them, and (b)
126 the self-diffusion coefficients of deuterium (D_2O or HDO), tritium (HTO) and ^{18}O ($^{18}\text{OH}_2$)
127 differ by as much as 10%. At the pore scale, one would thus naturally expect differences, as the
128 underlying transport process is essentially advective-diffusive. At larger scales, one can observe
129 either Fickian or non-Fickian transport. Fickian transport reflects, as already stated, the
130 asymptotic case of perfect mixing, characterized by normally distributed transport distances in
131 line with the advection-dispersion equation. However, the time scale for diffusive mixing
132 between flow lines grows with a declining diffusion coefficient of a tracer dispersion coefficient
133 grows with the inverse of the molecular diffusion coefficient, as detailed in section 2.1. We thus
134 argue that; Differences differences in self-diffusion coefficients of water isotopes should hence
135 affect dispersion and thus the variance of travel times, with slower diffusion causing larger
136 variances. However, in case of perfect mixing one would not expect differences in average
137 travel times, because for advective-dispersive transport the latter is controlled solely by the
138 average fluid velocity-, which This in turn does not dependent on molecular diffusion ~~or not~~
139 on the dispersion coefficient.

140
141 Here we conjecture that in the case of imperfect mixing, the average travel time becomes
142 sensitive to differences in diffusion coefficients *as well*, as detailed in section 2.1. Anomalous
143 transport can manifest through skewed travel distance distributions leading to a faster first
144 arrival and/or a longer tailing compared to Fickian transport (Levy and Berkowitz, 2003; Ederly

hat formatiert: Hervorheben

hat formatiert: Hervorheben

hat formatiert: Hervorheben

hat formatiert: Hervorheben

hat formatiert: Hervorheben, Hervorheben

hat formatiert: Hervorheben

hat formatiert: Hochgestellt, Hervorheben

hat formatiert: Hervorheben

hat formatiert: Hervorheben

hat formatiert: Hervorheben

hat formatiert: Hervorheben

hat formatiert: Hervorheben

hat formatiert: Hervorheben

hat formatiert: Hervorheben

hat formatiert: Hervorheben

hat formatiert: Hervorheben

hat formatiert: Hervorheben

hat formatiert: Hervorheben

145 et al., 2014; Edery et al., 2015; Dentz et al., 2023). Recent experimental work of Elhanati et al.
146 (2025) investigating the breakthrough of deuterium and Br^- through saturated columns
147 containing uniform and heterogeneous arrangements of porous media revealed very similar
148 behavior of both tracers, and quantitative analysis demonstrated clearly non-Fickian transport
149 with long tailing of breakthrough curves. Motivated by these findings and the discussion
150 between Stewart et al. (2010, 2021) and Rodriguez et al. (2021), we use physically based
151 numerical simulations to test our conjecture. To this aim, we explore the sensitivity of **average**
152 travel **times-time distributions** to the changes in **self**-diffusion coefficients, comparing transport
153 of tritium (**HTO**), deuterium (**HDO**), and $^{18}\text{OH}_2$ through media with different types and levels
154 of heterogeneity.

hat formatiert: Tiefgestellt

156 2 BACKGROUND AND NUMERICAL SIMULATIONS

157 2.1 Background: Solute transport in porous media in a nutshell

158 Before detailing the numerical experiments, we briefly revisit the theory of dissolved matter
159 transport, to justify our conceptual and numerical simulation approach. In the simplest case,
160 i.e., dissolved transport of an inert (non-reactive, conservative) substance through a fluid at rest
161 is solely controlled by molecular diffusion. According to Fick's law, the solute flux \mathbf{j} ($\text{kg s}^{-1} \text{m}^{-2}$)
162 is the product of the molecular diffusion coefficient, D_{mol} ($\text{m}^2 \text{s}^{-1}$), and the gradient in solute
163 concentration, C (kg m^{-3}):

$$164 \mathbf{j} = -D_{mol} \nabla C \text{ (Eq.1).}$$

167 Einstein (1905) showed that molecular diffusion is an effective, macroscopic fingerprint of
168 Brownian motion. Molecular diffusion (D_{mol}) grows with the absolute temperature but
169 decreases with **the-increasing** viscosity of the fluid and **the-increasing** diameter of the molecule.
170 Moreover, it is well known that for a fluid at rest and assuming an initial delta distribution of
171 the substance, the travel distance obeys Gaussian distribution, centered at the origin (Einstein,
172 1905). The variance of travel distance grows linearly with time t (s), while the molecular
173 diffusion coefficient is the growth factor.

174
175 When the fluid moves with constant and spatially homogeneous velocity, \mathbf{v} (m s^{-1}), the solute
176 flux is the sum of an advective and a diffusive component:

177
178
179
180
181
182
183
184
185
186
187
188
189
190
191
192
193
194
195
196
197
198
199
200
201
202
203
204
205
206
207
208

$$\mathbf{j} = \mathbf{v}C - D_{mol} \nabla C \text{ (Eq. 2).}$$

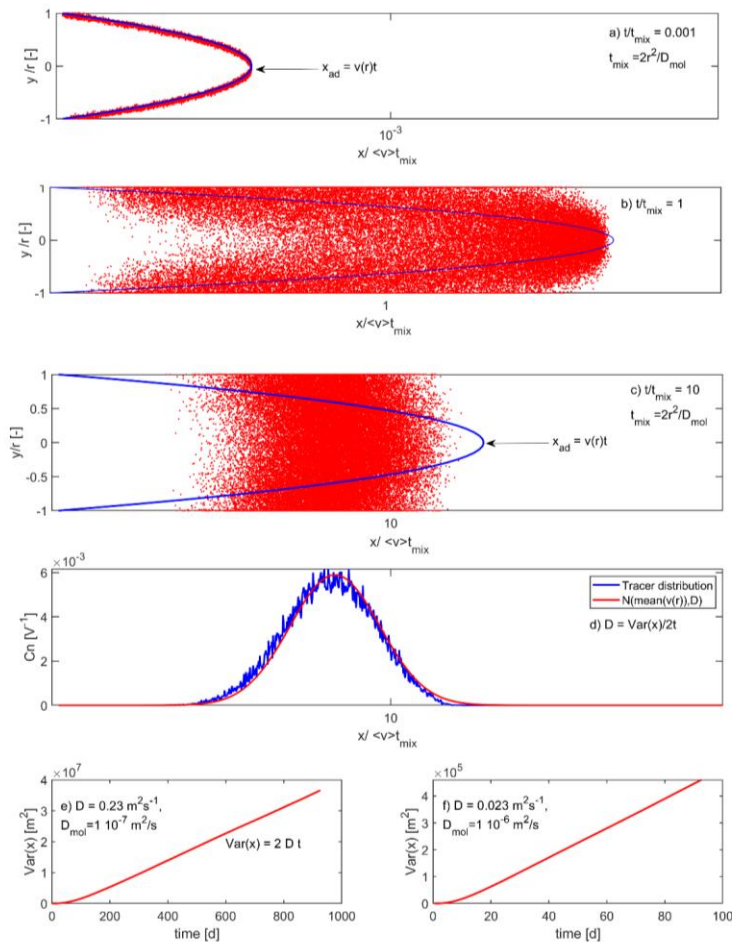
This is what is meant when loosely stating that the “solute velocity” is not equal to the fluid velocity. The distribution of travel distances still obeys Gaussian behavior, its variance increases proportionally to D_{mol} and t , while the mean travel distance grows with $\mathbf{v} t$. This is the well-known case of advection-diffusion.

In line with Einstein’s argument and Roth and Hammel (1996), we note that dispersion is a macroscopic, effective fingerprint of lateral diffusive mixing of solutes between flowlines of different fluid velocities. Recalling that water flow in an individual soil pore can be characterized by Hagen-Poiseuille law, this can be effectively visualized by discussing the migration of a tracer pulse injected into a pore of radius r (m) and travelling through the parabolic velocity field. Fig. 1 displays the three main states of Taylor-Aris dispersion, which were all inferred from particle tracking simulations (see section 2.2) through a parabolic flow field with mean velocity of $v = 10^{-4}$ m/s. For times t much smaller than the diffusive mixing time scale, $t_{mix} = \frac{2r^2}{D_{mol}}$, tracer molecules migrate along the same flowline and their displacement mirrors essentially the parabolic flow field (Fig. 1a). In this so-called near field, transport is essentially deterministic and the variance in travel distance scales with t^2 , as shown in Figs. 1e and 1f for small transport times. However, the non-uniform displacements in x directions cause a transversal concentration gradient between the flowlines, which is gradually depleted by transversal diffusive mixing from fast to slow flowlines and *vice versa* (see Fig. 1b for $t = t_{mix}$). For times much larger than the diffusive mixing time, all molecules experience the entire velocity field many times and the central limit theorem applies (Fig. 1 c).

The comparison of the travel distance distribution inferred from the particles to the Gaussian distribution in Fig. 1c corroborates that indeed a Gaussian travel time distribution emerges. The mean travel distance grows with the spatially averaged fluid velocity, \bar{v} , and t (Fig. 1d). The variance of travel times now grows linearly with t and the slope is the macro-dispersion coefficient D (Fig. 1e,f). For Taylor-Aris dispersion in a cylindrical pore with radius r , the dispersion coefficient shows the following dependency:

$$D \sim \frac{\overline{v^2} r^2}{D_{mol}} \text{ (Eq. 3)}$$

The key point is that D grows linearly with D_{mol}^{-1} . Fig. 1 corroborates for the simulated transport of two different tracers with D_{mol} of 1×10^{-7} (Fig. 1e) and 1×10^{-6} m²/s (Fig. 1f). Diffusion that is slower by a factor of 10 causes not only a ten times larger dispersion coefficient: it also implies that it takes ten times longer to reach the well-mixed advective-dispersive case and that the variance in travel distances increases ten times faster with time.



209

210

211

212

213

214

215

216

217

218 Figure 1: The three stages of Taylor-Aris dispersion in a capillary tube pore with radius r (m) as a function of the
 219 diffusive mixing time scale $t_{mix} = 2r/D_{mol}$: (a) near field for $t \ll t_{mix}$, intermediate state for $t = t_{mix}$ (b) and well mixed
 220 far field for $t \gg t_{mix}$ (c). Variance of particle transport distances as a function of time for $D_{mol} = 1 \times 10^{-6} \text{ m}^2/\text{s}$ (e)
 221 and $D_{mol} = 1 \times 10^{-7} \text{ m}^2/\text{s}$ (f). All graphs were inferred from transport simulations based on particle tracking.
 222

223 Of course, we acknowledge that dispersion in a real-world porous medium relates to the
 224 variability in pore sizes and that the geometry and tortuosity of soil pores is clearly more
 225 complex than the above example. **Naturally, this implies that dispersion in a porous medium**
 226 **shows a qualitatively different behavior. In one dimension, the dispersion coefficient is**
 227 **proportional to the product of the average flow velocity, v_x (not v_x^2), and the dispersivity of the**
 228 **porous medium. The latter characterizes the length scale of heterogeneities (Bear, 1972; Dentz**
 229 **et al., 2023). Yet we argue that Taylor dispersion and Hagen-Poiseuille flow occur in each**
 230 **individual soil pore. This implies the lateral diffusive mixing times for isotopic tracers will be**
 231 **different be due to their different self-diffusion coefficients, in each individual soil pore,**
 232 **meaning that that we expect the tracer with lower diffusion coefficient will experience a**
 233 **stronger longitudinal dispersion. When a well defined We thus conjecture advective dispersive**
 234 **transport process emerges, we expect that the variance of travel distances and travel times will,**
 235 **hence nevertheless, grow with the decreasing molecular diffusion coefficient. However in the**
 236 **case of perfect mixing, we do not expect that different isotopes will show different mean travel**
 237 **times, simply because advective-dispersion transport relies on a linear superposition of**
 238 **advective and dispersive solute flux, and the average flow velocity \bar{v}_x is not affected by changes**
 239 **in the self-diffusion coefficient.**

$$241 \quad j = \overset{\text{advective solute flux}}{\bar{v}C} - \overset{\text{dispersive solute flux}}{D\nabla C} \quad (\text{Eq. 4}).$$

242
 243 Instead, we propose that the independence of the average transit time from the self-diffusion
 244 coefficient no longer holds when non-Fickian transport occurs. The latter breaks the symmetry
 245 of ~~perfect mixing~~ **the Gaussian travel distance distribution** (Bloschl and Zehe, 2005), ~~either~~
 246 because molecules are ~~either~~ trapped in low conductive bottlenecks for very long times, and/or
 247 ~~are because molecules~~ traveling along rapid preferential flow paths ~~leave~~ **leaving** the system
 248 after very short times (Berkowitz and Zehe, 2020; Wienhöfer et al., 2009). As an important
 249 implication **of the long tailing**, the travel time distribution becomes skewed and in the case of
 250 advective trapping in low conductive bottlenecks, one might expect that an isotope with a

hat formatiert: Hervorheben

hat formatiert: Hervorheben

hat formatiert: Hervorheben

hat formatiert: Hervorheben

hat formatiert: Hervorheben

hat formatiert: Hochgestellt

hat formatiert: Hervorheben

hat formatiert: Hervorheben

hat formatiert: Hervorheben

hat formatiert: Hervorheben

hat formatiert: Hervorheben

hat formatiert: Hervorheben

hat formatiert: Hervorheben

hat formatiert: Hervorheben

251 smaller self-diffusion coefficient stays in the bottlenecks for longer times compared to an
252 isotope which exhibits faster diffusion. This could imply that in case of as for non-Fickian
253 transport average transit times grow with a decreasing self-diffusion coefficient.
254

255 2.2 Transport simulations and numerical experiments

256 To shed light on the role of the different self-diffusion coefficients of deuterium, tritium and
257 O¹⁸ for the average-transit time distributions, we simulated advective-diffusive transport
258 through steady-state flow fields in 2d-two dimensional saturated domains of increasing
259 heterogeneity, comparing the transport of the three different water isotopes. Their respective
260 self-diffusion coefficients in water at a temperature of 25 °C are, according to Devel (1962) and
261 Wang (1952), $D_{\text{HDO}} = 2.25 \times 10^{-9} \text{ m}^2 \text{ s}^{-1}$, $D_{\text{HTO}} = 2.44 \times 10^{-9} \text{ m}^2 \text{ s}^{-1}$ and $D_{\text{18OH2}} = 2.66 \times 10^{-9} \text{ m}^2 \text{ s}^{-1}$. For the case of HTO we chose to ignore its radioactive decay, to assure that optional
262 differences in average travel times stem only from the differences in self-diffusion coefficients.
263

264
265 In all investigated cases we used particle tracking to simulate isotope transport in combination
266 with the respective flow fields. The particle advancement, Δs (m), being characterized by the
267 Langevin equation, starting from a given particle location at time t_i :

$$268 \Delta \mathbf{s}(x, y) = \mathbf{v}[\mathbf{s}(t_i)]\Delta t + \xi \sqrt{2 D_{mol} \Delta t} \quad (\text{Eq. 5})$$

269
270
271 The first term characterizes advective displacement, depending on the 2d fluid velocity vector
272 \mathbf{v} , and the time step Δt . The second term denotes the diffusive displacement, which scales with
273 a modulus of $\sqrt{2 D_{mol} dt}$ times a standard normally distributed random number ξ .

274
275 Three different model scenarios, A, B, and C, are examined, accounting for different types of
276 hydraulic conductivity fields and heterogeneities. In all cases tested, the dependence of the
277 simulations on the chosen number of particles compared $N=10^4$, 5×10^4 , 10^5 and 2×10^5 ; results
278 were independent of N at particle numbers larger than 10^5 . In all cases fluid velocities were
279 interpolated to the particle position using inverse distance weighting.

280 **2.2.1 Scenario A: Isotope transport through a homogeneous medium with an**
281 **embedded lower permeable lens**

282 Scenario A was inspired by the experimental work of Elhanati et al. (2025) investigating the
283 breakthrough of deuterium and Br- through homogeneous, (uniformly packed) ~~and~~
284 ~~heterogeneous~~ sand columns and sand columns with an embedded lower permeable lens (Fig.
285 2, Scenario A). We simulated steady flow through a 1 m by 10 m block using the following
286 configurations:

- 287 • A1.1) a sandy saturated soil with hydraulic conductivity $K_s=1 \times 10^{-5}$ m/s and porosity of
288 0.4, surrounding a less conductive lens (Fig. 2) with hydraulic conductivity of $K_s=10^{-9}$
289 m/s.
- 290 • A.1.2) same configuration as A1.1), while the less conductive lens has a hydraulic
291 conductivity of $K_s=10^{-8}$ m/s
- 292 • A2.1) a saturated loess soil with hydraulic conductivity $K_s=1 \times 10^{-7}$ m and porosity of
293 0.46, surrounding a less conductive lens (Fig. 2) with hydraulic conductivity of $K_s=10^{-9}$
294 m/s.
- 295 • A2.2) same configuration as A2.1), while the less conductive lens has a hydraulic
296 conductivity of $K_s=10^{-8}$ m/s.

297 In all cases, we used a discretization of 0.2 m by 0.2 m, a permeameter type of boundary
298 condition with a head gradient of 0.05 m/m, and calculated the flow field using the model
299 CATFLOW (Zehe et al. 2001). CATFLOW is a physically based model to simulate the
300 water balance and subsurface transport at hillslope scale. CATFLOW simulates subsurface
301 water dynamics based on the ~~potential based~~ two dimensional Darcy-Richards equation
302 using curvilinear orthogonal coordinates. The equation is solved using a mass conservative
303 Picard iteration (Celia et al., 1990) with adaptive time stepping. While the model also
304 accounts ~~additionally also~~ for overland flow, evaporation and transpiration and solute
305 transport, we omit details here; as we ~~solely~~ make use ~~solely~~ of the simulated steady state
306 flow fields. ~~These flow fields~~ were generated ~~We considered using no-flow~~ boundary
307 conditions on the horizontal domain boundaries. Using these flow fields, ~~We~~ we simulated
308 advective diffusive transport by ~~using means of~~ particle tracking according to Eq. 5 and
309 time steps of 1 h and ~~10⁵ a particles~~ number of ~~10⁵~~. -As scenario A is partly an upscaled
310 version of the medium that Elhanati et al. (2025) used in their experiments, we expect that
311 non-Fickian transport will emerge in line with their experimental findings. However, it was

Formatiert: Einzug: Links: 0,5 cm, Erste Zeile: 0 cm, Mit Gliederung + Ebene: 3 + Nummerierungsformatvorlage: 1, 2, 3, ... + Beginnen bei: 1 + Ausrichtung: Links + Ausgerichtet an: 1,5 cm + Tabstopp nach: 2,77 cm + Einzug bei: 2,77 cm, Tabstopps: Nicht an 2,77 cm

hat formatiert: Hervorheben

hat formatiert: Hervorheben

hat formatiert: Hervorheben

hat formatiert: Hervorheben

hat formatiert: Hervorheben

hat formatiert: Hervorheben

hat formatiert: Hervorheben

hat formatiert: Hervorheben

hat formatiert: Hervorheben

hat formatiert: Hervorheben

hat formatiert: Hervorheben

hat formatiert: Hervorheben

hat formatiert: Hervorheben

hat formatiert: Hervorheben

hat formatiert: Hervorheben

hat formatiert: Hervorheben

hat formatiert: Hervorheben

hat formatiert: Hervorheben

hat formatiert: Hervorheben

hat formatiert: Hervorheben

hat formatiert: Hervorheben

not possible to reconstruct the exact hydraulic conductivities of these experiments, so that we expect similar qualitative behavior but not a one-to-one correspondence.

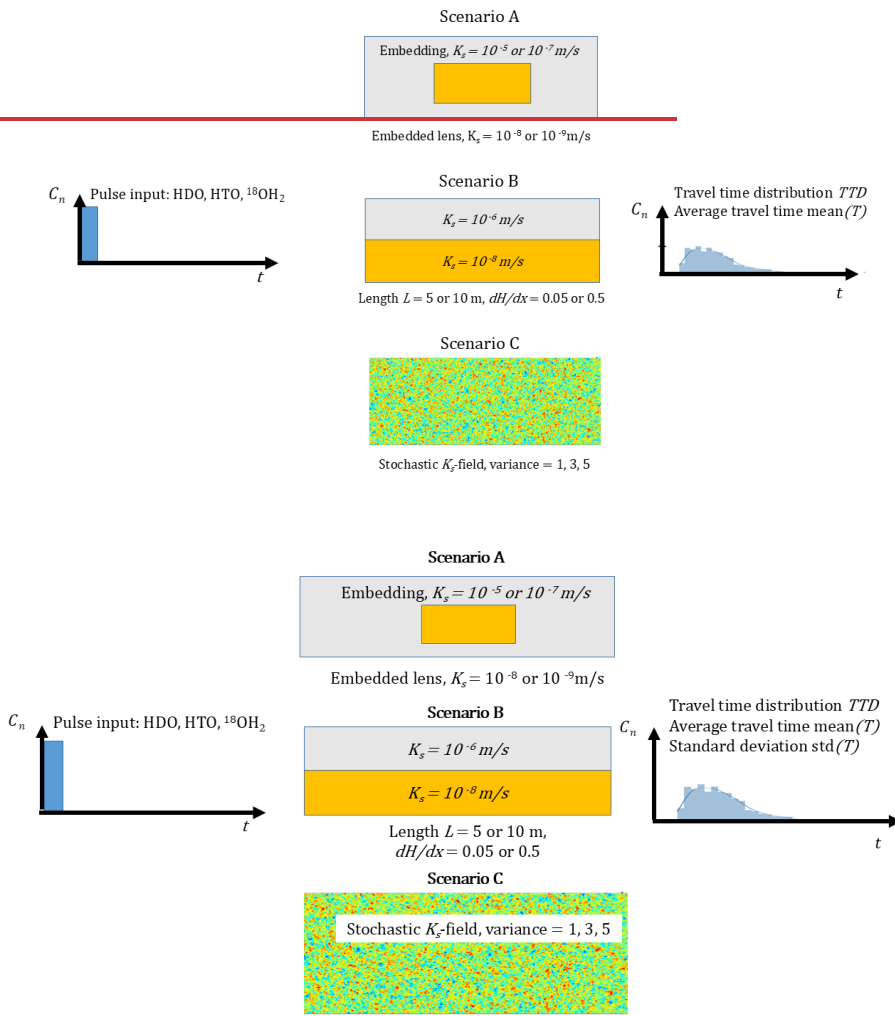


Figure 2: Scheme of model scenarios.

2.2.2 Scenario B: Isotope transport through a two-layered aquifer at different head gradients

Formatiert: Einzug: Links: 0,5 cm, Erste Zeile: 0 cm, Mit Gliederung + Ebene: 3 + Nummerierungsformatvorlage: 1, 2, 3, ... + Beginnen bei: 1 + Ausrichtung: Links + Ausgerichtet an: 1,5 cm + Tabstopp nach: 2,77 cm + Einzug bei: 2,77 cm, Tabstopps: 1,27 cm, Listentabstopp + Nicht an 2,77 cm

321 In scenario B, we simulated advective-diffusive solute transport in a simple two-layer aquifer
322 system of 2 m total height ~~and a length of either 5 or 10 m (Fig. 2, Scenario B) and a length of~~
323 ~~either 10 m (B1) or 5 m (B2)~~. The layers with a height of 1m are homogeneous but differ by
324 their saturated hydraulic conductivity ~~of~~ $K_s=10^{-6}$ m/s and $10^{-8.8}$ m/s. Both layers were exposed
325 to the same head gradient, which was first set to $dH/dx = 0.05$ and then to $dH/dx = 0.5$ to
326 compare ~~overall two-four~~ different Peclet numbers. Transport of deuterium, tritium and ^{18}O
327 with their ~~self~~-diffusion coefficients was simulated using a pulse input of ~~100,000~~ 10^5 particles
328 through the left upstream domain, while no-flow conditions were assigned to the two horizontal
329 domain boundaries. ~~Time stepping was set to one hour.~~

hat formatiert: Hochgestellt

331 2.2.3 Scenario C: Isotope transport through a stochastic heterogeneous aquifer 332 with increasing variance in hydraulic conductivity

333 In scenario C (Fig. 2, Scenario C; Fig. 3), we ~~considered-revisited~~ steady-state fluid flow within
334 two-dimensional, stochastic heterogeneous media with moderate ($\text{var} = 1$), intermediate (var
335 $= 3$) and strong variance ($\text{var} = 5$) in the hydraulic conductivity ~~(from the study of Zehe et al.,~~
336 ~~(2021)~~. The 60 m long and 20 m wide domain was discretized into 0.2 m by 0.2 m elements.
337 Flow was driven by ~~a total head gradient of difference~~ $\Delta H = dH/dx = 1/610$ m, from the left
338 upstream boundary to the right downstream boundary, while no-flow conditions were assigned
339 to the two horizontal domain boundaries. We used random and yet statistically homogeneous,
340 isotropic Gaussian fields of three different variance of $\ln(K)$, namely 1, 3 and 5 generated with
341 the sequential Gaussian simulator GCOSIM3D (Gómez-Hernández et al., 1997) and a
342 correlation length of 1 m. Advective diffusive transport was again simulated using particle
343 tracking according to Eq. 5.

hat formatiert: Schriftart: Symbol, Kursiv

hat formatiert: Schriftart: Kursiv

344 ~~Our Previous-previous~~ work showed that these media were highly susceptible to preferential
345 flow and transport, ~~while one could observe a stronger funneling into preferential flow paths~~
346 ~~with increasing variance (Edery et al., 2014; Zehe et al., 2021)-), as visualized in Fig. 3-. For~~
347 ~~the particle tracking we compared-used simulations-simulated flow fields for an average~~
348 ~~hydraulic conductivity of $K_s = 10^{-7}$ m/s or $K_s = 10^{-6}$ m/s to account for two different Peclet~~
349 ~~numbers-, injecting 10^5 particles at the upstream left boundary and using hourly time steps. Fig.~~
350 ~~3 shows the hydraulic conductivity fields and the cumulative number of particles that visited a~~
351 ~~grid cell in the simulation domain for small, medium and large variance for the lower average~~
352 ~~hydraulic conductivity.~~

hat formatiert: Hervorheben

hat formatiert: Hervorheben

hat formatiert: Hervorheben

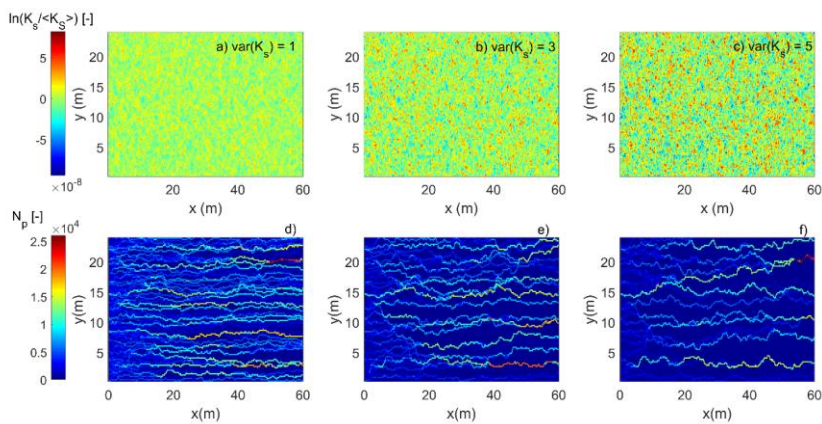
hat formatiert: Hervorheben

hat formatiert: Hervorheben

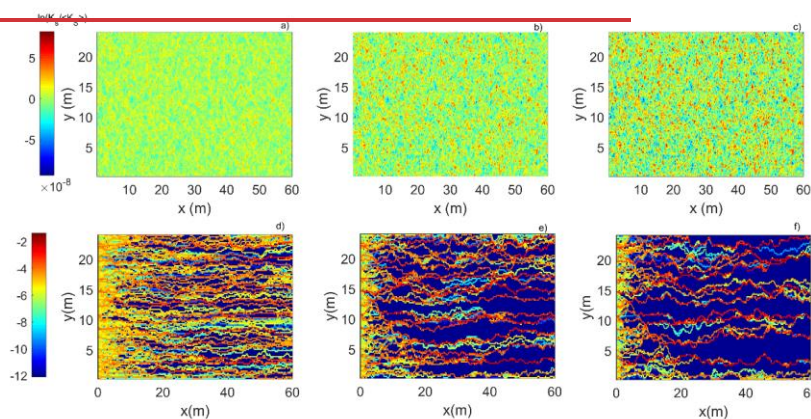
hat formatiert: Hervorheben

hat formatiert: Hochgestellt, Hervorheben

hat formatiert: Hervorheben



355



356

357

358

359

360

361

Figure 3: The normalized hydraulic conductivity fields for three randomly selected realizations of small, medium and large variance (a, b, c). Normalized Cumulative-cumulative number of particles (N_p) that visited a grid cell in the simulation domain for small, medium and large variance (d, e, f) for HDO inferred from a critical flow path analysis. Funneling of water and HDO into preferred pathways become clearer stronger with increasing variance of the hydraulic conductivity field.

hat formatiert: Deutsch (Deutschland)

hat formatiert: Hervorheben

362

3 RESULTS

363

3.1 -Travel time distributions inferred from scenario A

364

While scenario 4 did not generally not yield distinct differences in the simulated travel time distribution for different isotopic tracers, we found for all scenarios travel time distributions with longer tails. Figure 4 shows this exemplarily for scenarios A 2.1 and A 2.2 (the Fig-4 shows the normalized breakthrough curves of deuterium for the heterogeneous case with the low conductive embedding-) by comparing their travel time distributions, derived from the

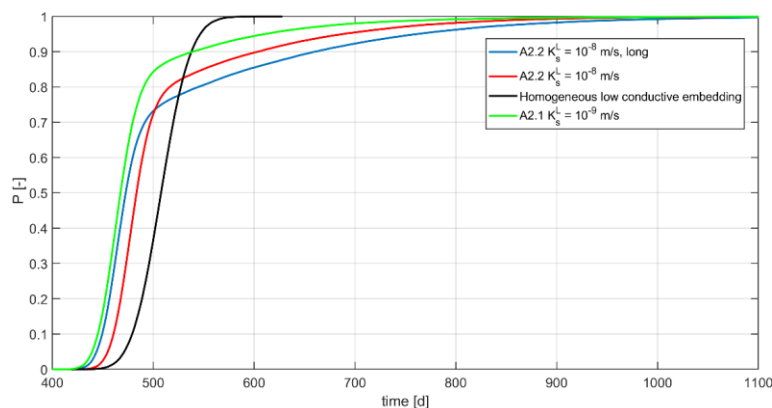
367

368

369 accumulated normalized breakthrough curves (CBTC), using the well mixed transport through
 370 the homogeneous medium without clays lens as well mixed, Gaussian reference. containing
 371 either a lower conductive or a higher conductive clay lens. This reveals, in line with the
 372 experimental evidence of Elhanati et al. (2025), a clearly non-Fickian breakthrough with travel
 373 time distribution with an earlier first arrival and a significantly longer tailing compared to the
 374 Gaussian reference breakthrough curve of the homogeneous system (green dots/black line, Fig.
 375 4). In addition, Fig. 4-Table 1 provides average-the mean travel time ($\text{mean}(T)$), named
 376 $\text{mean}(T)$'s standard deviation ($\text{std}(T)$), as well as the 10%, 20% 50%, 75% and 90% quantiles
 377 (T10, T25, T50, T75, T90). Case 2.1 (solid green) has clearly the smallest average travel time,
 378 due to the faster first arrival, while it has also a larger standard deviation and a longer tailing,
 379 compared to the Gaussian case. So here the earlier first arrival dominates against the longer tail.
 380 Mean travel times drop below that one of the Gaussian reference when increasing hereafter,
 381 which correspond to the first central moment of the normalized breakthrough curve. We find
 382 that the average travel times through the heterogeneous media are, with $\text{mean}(T) = 509.4, 510.3$
 383 and 515.4 d, larger than the average travel time through the homogeneous medium, which is
 384 $\text{mean}(T) = 508.4$ d. Interestingly, we observe that the average travel time declines slightly when
 385 the hydraulic conductivity of the clay lens is increased from 10^{-9} to 10^{-8} m/s (Fig. 4, solid red
 386 A.2.2), despite the earlier first arrival. The This latter can be explained by a stronger advective
 387 transport of the tracer into the lens, due to the smaller drop in conductivity. This clearly leads
 388 to a much longer tailing, which at the end ultimately controls the shift to larger mean travel
 389 times. Consistently, we observe an even larger mean(T)mean travel time of 515.4 d, when
 390 elongating the clay lens with $K_s = 10^{-8}$ m/s by 30% (Fig 4. A.2.2 long, solid blue).

hat formatiert: Schriftart: Kursiv

hat formatiert: Schriftart: Kursiv



392

Figure 4: Cumulative breakthrough curves/travel time distributions of HDO for scenario A.2.1 and A. 2.2, i.e., the low conductive embedding medium with $K_s = 10^{-7} \text{ m s}^{-1}$, using the travel time distribution through the homogeneous medium as reference.

Table 1: Mean travel time ($\text{mean}(T)$), its standard deviation ($\text{std}(T)$), as well as the 10%, 20% 50%, 75% and 90% quantiles (T10, T25, T50, T75, T90) for cases shown in Fig. 4. For convenience we included the hydraulic retention time, RT_{hyd} .

Case	RT_{hyd} [d]	$\text{mean}(T)$ [d]	$\text{std}(T)$ [d]	T10 [d]	T25 [d]	T50 [d]	T75 [d]	T90 [d]
A 2.1	507.0	485.0	64.9	445.1	455.2	467.0	484.2	539.2
A 2.2	506.9	510.4	81.7	460.0	470.1	483.1	503.1	603.1
A 2.2, long	509.1	515.4	109.1	449.1	459.0	472.2	507.3	660.3
Homogen.	508.4	508.3	22.9	47.09	492.5	508.2	523.2	537.5

For convenience, we compared the average travel times, mean travel time, $\text{mean}(T)$, to the average hydraulic retention time, RT_{hyd} , which was calculated by dividing the total pore volume of the domain by the averaged flow rate. RT_{hyd} and $\text{mean}(T)$ match, as expected, naturally very well for the case of Fickian transport through the homogeneous domain. In the case of non-Fickian transport, however, we observe that the average travel times inferred from the CBTCs are slightly larger than suggested by deviate from the hydraulic retention time RT_{hyd} . In case 2.1 it is actually smaller, while in case 2.2 it is slightly larger. This underestimate grows clearly with the length and thickness of the BTC tails.

We generally acknowledge that one can *a priori* expect deviations from Fickian transport in this setup scenario A, as the transport distance is only twice as large as the length of the embedded clay lens. Yet, the long tail reflects diffusion of molecules into the low conductive lens, which evidently reside there for considerably long times. The channeling of the flow around the lens and the enlarged transport velocities explain in turn the earlier arrival of the solutes compared to the homogeneous case. However, we did not find variations in any of the average travel times that related to the different self-diffusion coefficients of the isotopic tracers.

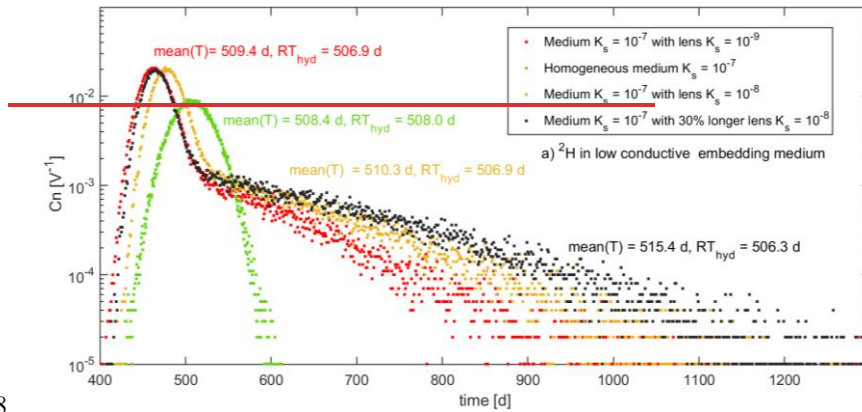


Figure 4: Normalized breakthrough curves of HDO and related average travel times TTD and hydraulic retention times for scenario A for the low-conductive embedding medium with $K_s = 10^{-7} \text{ m s}^{-1}$.

3.2 Travel time distributions inferred from scenario B

Fig. 5 provides the cumulative ~~normalized~~ breakthrough curves/travel time distributions (TTD) ~~for~~ through the two layered case B through the 10 (Fig. 5a, c) and 5 m long layered aquifer (Fig. 5b, d), as a function of the two different head gradients, system of 10 m (B1) and 5 m length (B2) at the two different head gradients. In all cases we found a distinct dependence of the TTD on the self-diffusion coefficient of the different isotopes. Generally, HDO exhibits in all cases the largest mean travel time followed by HTO followed by $^{18}\text{OH}_2$ (Table 2). A slower self-diffusion implies indeed a shift towards longer travel times, which manifest particularly in the long tails and the larger quantiles (Table 2). To highlight these differences, Fig. 5 zooms to travel times larger than the 80% quantiles and smaller than 99% quantiles. We found however also that the standard deviation and thus the dispersion of travel times grows systematically with declining self-diffusion coefficient.

hat formatiert: Nicht Hochgestellt/ Tiefgestellt

$^{18}\text{OH}_2$	2.47	4.04	0.28	0.3	0.32	1.53	6.83
B2.2 (5 m)	dH/dx =	0.05	Pe = 1.1				
HDO	8.91	10.09	2.73	3.08	4.02	10.62	22.2
HTO	8.62	9.52	2.72	3.09	4.07	10.48	20.93
$^{18}\text{OH}_2$	8.41	8.95	2.71	3.11	4.14	10.39	20.36

447 The median travel times in Table 2 grow for both large head gradients almost linearly with
448 transport distance, from app. 4 to 9 years (for the small gradient) 0.32 to app. 0.65 y (for the
449 large gradient). However, for each travel distance, driving head and isotope the mean travel
450 time is minimum two and maximum five times larger than the corresponding median, which
451 underlines that TTD are strongly skewed due to very long tails. Absolute differences between
452 mean travel times are largest comparing HDO. Average travel times range from the order of
453 700 d to the short aquifer at the high Peelet (Fig. 5b) to the order of 5300 d for the longer aquifer
454 and the smaller Peelet (Fig. 5c) and $^{18}\text{OH}_2$. They appear largely independent from the length of
455 the aquifer ranging from app. 0.2 y for the larger head gradient to app. 0.5 y- for the gradient.
456 The corresponding relative differences decline naturally with increasing length of the aquifer
457 ranging from 7% to 4%. Interestingly, we can observe a rather stable relative difference between
458 the standard deviation of travel times of HDO and $^{18}\text{OH}_2$ of approximately 10%, which implies
459 that differences in their variance and thus dispersion are approximately 20%. This relative
460 difference corresponds nicely well to the relative difference between the self-diffusion
461 coefficients of $D_{\text{HDO}} = 2.25 \times 10^{-9} \text{ m}^2 \text{ s}^{-1}$ and $D_{^{18}\text{OH}_2} = 2.66 \times 10^{-9} \text{ m}^2 \text{ s}^{-1}$. A closer look reveals
462 that while the breakthrough curves of the three tracers look similar, their corresponding first
463 central moments are indeed different, as shown in the legend of Fig. 5. One can see a clear
464 increase of the average travel time with a declining diffusion coefficient of the isotopic tracers.
465 Deuterium has the smallest self diffusion coefficient but generally the longest average travel
466 time, while it is *vice versa* for ^{18}O . For a better comparison we focus on the difference between
467 the average travel time of deuterium and ^{18}O , defined as:

$$470 \text{ dTT} = \text{mean}(T_{\text{HDO}}) - \text{mean}(T_{^{18}\text{OH}_2}) \text{ (Eq. 6);}$$

471 and the relative difference thereof, defined as:

$$474 \text{ dTT}_{\text{rel}} = \text{dTT} / \text{mean}(T_{^{18}\text{OH}_2}) \text{ (Eq. 7);}$$

hat formatiert: Schriftart: Times New Roman, 10 Pt.,
Schriftfarbe: Grün, Hochgestellt

hat formatiert: Schriftart: Times New Roman, 10 Pt.,
Schriftfarbe: Grün

hat formatiert: Schriftart: Times New Roman, 10 Pt.,
Schriftfarbe: Grün, Tiefgestellt

hat formatiert: Schriftart: Times New Roman, 10 Pt.,
Schriftfarbe: Grün

hat formatiert: Schriftart: Times New Roman, 10 Pt.,
Schriftfarbe: Grün

Formatiert: Zentriert

hat formatiert: Schriftart: Times New Roman, 10 Pt.

hat formatiert: Schriftart: Times New Roman, 10 Pt.

hat formatiert: Schriftart: Times New Roman, 10 Pt.

hat formatiert: Schriftart: Times New Roman, 10 Pt.

Formatiert: Zentriert

Formatiert: Zentriert

hat formatiert: Schriftart: Times New Roman, 10 Pt.,
Schriftfarbe: Blau

Formatiert: Zentriert

hat formatiert: Schriftart: Times New Roman, 10 Pt.,
Schriftfarbe: Akzent 2

Formatiert: Zentriert

hat formatiert: Schriftart: Times New Roman, 10 Pt.,
Schriftfarbe: Grün, Hochgestellt

hat formatiert: Schriftart: Times New Roman, 10 Pt.,
Schriftfarbe: Grün

hat formatiert: Schriftart: Times New Roman, 10 Pt.,
Schriftfarbe: Grün, Tiefgestellt

hat formatiert: Schriftart: Times New Roman, 10 Pt.,
Schriftfarbe: Grün

Formatiert: Zentriert

hat formatiert: Hochgestellt

hat formatiert: Tiefgestellt

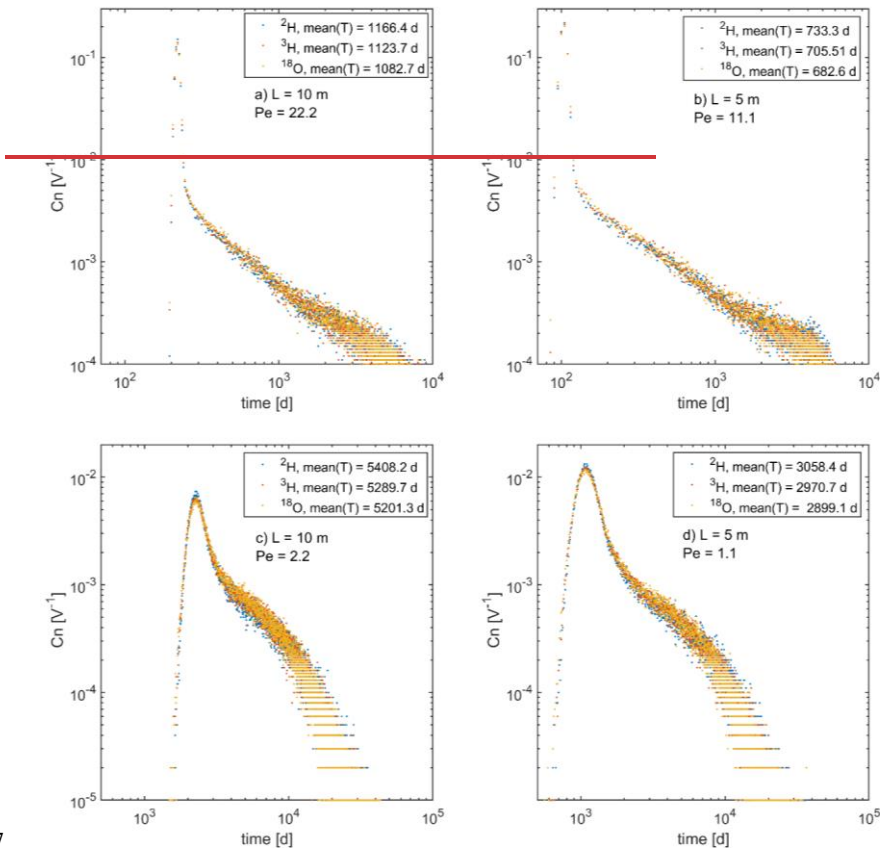
hat formatiert: Tiefgestellt

Formatiert: Block

Formatiert: Block

476 dTT increases with the length of the system but declines with the Peclet number. Differences
 477 in mean travel times, dTT , range from 51 d for the short aquifer and the high Peclet number of
 478 11.1 (Fig. 5b) up to 207 days for the longer aquifer and the small Peclet number of 2.2 (Fig.
 479 5c). Note that the relative differences dTT_{rel} are small: app. 5% for the small Peclet and they
 480 increase to 10% when increasing the Peclet number.

481
 482 For both aquifers, we calculated again the hydraulic retention times, using the arithmetic and
 483 the geometric means of the hydraulic conductivities of the layers, respectively. The latter was,
 484 for the hydraulic gradient of the small Peclet number with $RT_{hyd} = 1557$ d (4.2 y), more than
 485 three times smaller than the average travel times inferred from the tracer breakthrough curves,
 486 which was of order 5300 d (Fig. 5c).



487

488 Figure 5: Normalized breakthrough curves of deuterium (^2H blue dots), tritium (^3H red dots) and ^{18}O (yellow dots)
 489 and the corresponding average travel times, $\text{mean}(T)$, for scenario B. Simulations for the 10 m (a, c) and 5 m (b,
 490 d) long layered aquifer, for the two head gradients and the corresponding Peclet numbers (Pe). Note that for better
 491 visibility panels a and b, as well as c and d, have different scales.

492 The corresponding difference for the shorter aquifer and the high Peclet number is smaller but
 493 still remarkable: RT_{hyd} is with 578.5 d more than a 100 d smaller than the average travel times
 494 inferred from the particle transport simulations. This underpins that even in the case of simple
 495 layered systems, the analysis of hydraulic retention times may, due to the difference between
 496 fluid and tracer velocities, yield error prone estimates of average tracer travel times.

497 3.3 Travel time distributions inferred from scenario C

498 Fig. 6 presents the normalized breakthrough and average travel times $\text{mean}(T)$ distributions for
 499 scenario C for all isotopic tracers for all isotopic tracers, variance in hydraulic conductivity
 500 grows from the top to the bottom rows, cases with $\text{mean}(K_v) = 1 \times 10^{-6}$ m/s appear in left
 501 column, those with $\text{mean}(K_v) = 1 \times 10^{-7}$ m/s appear in the right column. In all cases except
 502 C1.1, there is a distinct dependence of the TTD on the self-diffusion coefficient. Generally,
 503 HDO exhibits the largest mean travel time followed by HTO followed by $^{18}\text{OH}_2$ (Table 3). The
 504 TTD of C.1.1 ($\text{var}=1, \text{mean}(K_v) = 1 \times 10^{-6}$) is very close to the well mixed case, as the mean and
 505 median travel times is are for all isotopes very similarelose. Differences in mean and median
 506 travels generally grow generally when moving to larger variances, while differences in travel
 507 time distributions become more, more distinct particularly in the 75% and 90% quantiles (Table
 508 3) and the tails (Fig. 6).

509
 510 at transport distances of $L = 60$ m (a, c, e) and 30 m (b, d, f). The variance of the hydraulic
 511 conductivity field decreases from top to bottom panels, the average K_v is 10^{-7} m/s. The strength
 512 of the “transport anomaly,” i.e., its deviation from Gaussian behavior, clearly increases with
 513 the variance of the hydraulic conductivity field and increasing transport distance. The larger the
 514 variance, the longer the tail of the breakthrough curve. The average travel time to $L = 30$ m
 515 increases from approximately 1310 days for variance 1, up to approximately 1810 days for
 516 variance 5. Note that for $L = 60$ m the corresponding difference is of the order of 1000 days.
 517 Consequently, the average travel time of a tracer for a given transport distance L increases
 518 strongly with the variance of the hydraulic conductivity field. Table 3: Mean travel time ($\text{mean}(T)$),
 519 its standard deviation ($\text{std}(T)$), as well as the 10%, 20% 50%, 75% and 90% quantiles (T10, T25, T50, T75, T90)
 520 for cases shown in Fig. 6. The color coding corresponds to the plots of the different isotopes in Fig. app.

	$\text{mean}(T)$	$\text{std}(T)$	T10	T25	T50	T75	T90
--	------------------	-----------------	-----	-----	-----	-----	-----

hat formatiert: Nicht Hochgestellt/ Tiefgestellt

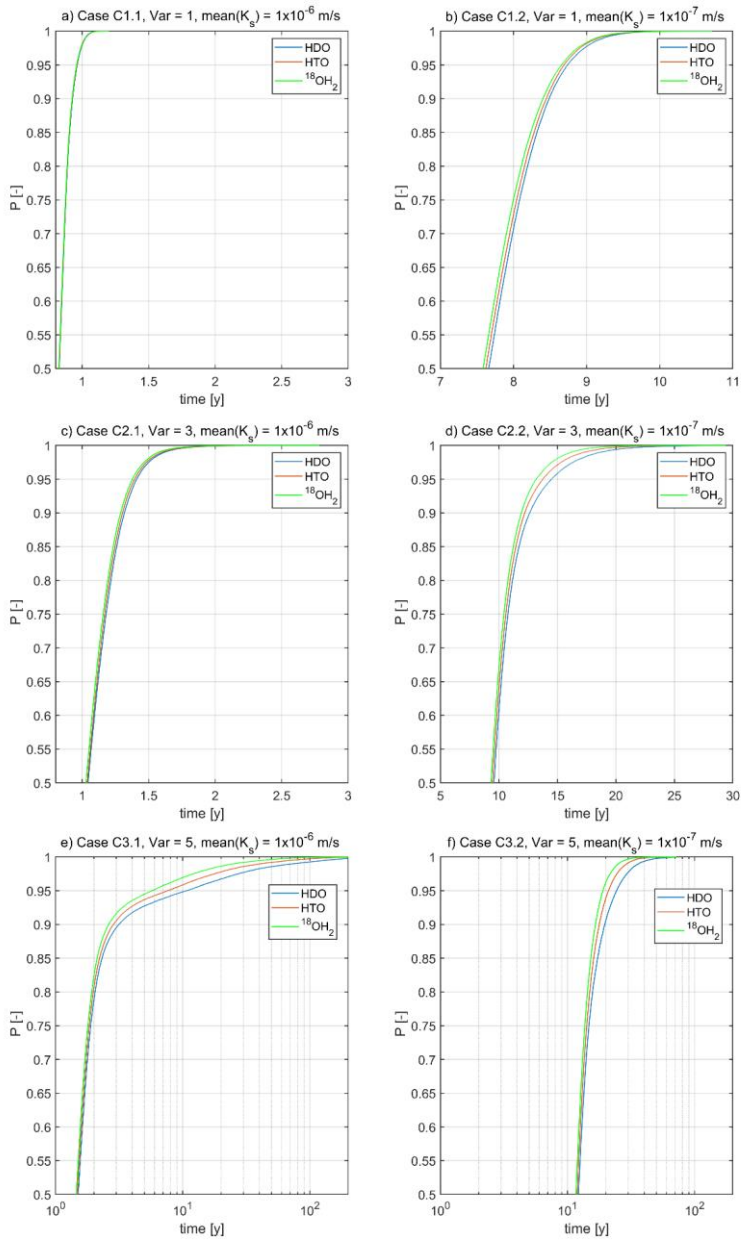
hat formatiert: Schriftart: Kursiv

hat formatiert: Schriftart: Kursiv

hat formatiert: Schriftart: Kursiv

hat formatiert: Schriftart: Kursiv

	[y]	[y]	[y]	[y]	[y]	[y]	[y]
C 1.1	Var = 1	Ks =	1×10^{-6} m/s				
HDO	0.832	0.074	0.740	0.781	0.828	0.877	0.927
HTO	0.831	0.073	0.739	0.780	0.827	0.876	0.926
¹⁸ OH ₂	0.829	0.073	0.738	0.779	0.824	0.874	0.924
C 1.2	Var = 1	Ks =	1×10^{-7} m/s				
HDO	7.671	0.621	6.893	7.238	7.644	8.068	8.482
HTO	7.632	0.613	6.863	7.208	7.605	8.030	8.430
¹⁸ OH ₂	7.598	0.609	6.833	7.175	7.573	7.989	8.389
C 2.1	Var = 3	Ks =	1×10^{-6} m/s				
HDO	1.064	0.198	0.827	0.923	1.041	1.178	1.315
HTO	1.056	0.194	0.825	0.921	1.036	1.167	1.301
¹⁸ OH ₂	1.046	0.190	0.819	0.912	1.027	1.156	1.288
C 2.2	Var = 3	Ks =	1×10^{-7} m/s				
HDO	10.076	2.243	8.019	8.690	9.575	10.767	12.627
HTO	9.861	2.018	7.918	8.570	9.441	10.592	12.211
¹⁸ OH ₂	9.678	1.842	7.819	8.469	9.318	10.427	11.918
C 3.1	Var = 5	Ks =	1×10^{-6} m/s				
HDO	3.824	13.637	1.058	1.244	1.504	1.888	3.140
HTO	3.066	9.735	1.052	1.230	1.477	1.838	2.849
¹⁸ OH ₂	2.457	5.952	1.038	1.214	1.452	1.792	2.608
C 3.2	Var = 5	Ks =	1×10^{-7} m/s				
HDO	13.736	5.4166	9.611	10.663	12.186	14.732	19.633
HTO	12.987	4.1824	9.4192	10.444	11.899	14.148	17.764
¹⁸ OH ₂	12.46	3.4702	9.2603	10.252	11.636	13.674	16.575



521
 522 **Figure 6: Travel time distributions of HDO (solid green), HTO (solid red) and $^{18}\text{OH}_2$ (solid blue) for scenario C:**
 523 **variance in hydraulic conductivity grows from the top to the bottom rows, cases with mean(K_s) = 1×10^{-6} m/s**
 524 **are appear in left column, those with mean(K_s) = 1×10^{-7} m/s are appear in the right column. For a better**

Formatiert: Zentriert

hat formatiert: Hochgestellt

hat formatiert: Hochgestellt

525 visualization of the main differences, we zoom to travel times larger than the median. Note that scaling of the
526 ordinates is different, color coding is consistent with Table 3.

527
528 ~~Remarkable~~Significant absolute differences in the mean travel times of HDO and $^{18}\text{OH}_2$ occur
529 for C2.2 (var =3, lower K_s) with approximately 0.4 y, and particularly for both cases with
530 variance of 5 (C3.1 and C.3.2) with absolute difference of approximately 1.4 y. ~~For~~The case
531 of the lower mean hydraulic conductivity ~~this~~ corresponds to a relative difference of 10%. For
532 the higher mean hydraulic conductivity we observe, however, that HDO (mean(T) = 3.83 y)
533 travels on average 50% slower than $^{18}\text{OH}_2$ (mean(T) = 2.46 y). The reason for this high relative
534 difference is that the 10 times higher conductivity leads ~~often~~ earlier first arrival while the
535 travel times ~~still exhibits~~ ~~show still~~ a very long tailing with substantial differences between the
536 isotopes. Note that for C3.1 differences in the mean travel time of HDO (mean(T) = 3.83 y) and
537 HTO (mean(T) = 3.1 y) are with approximately 0.75 y, substantially larger ~~clearly as~~ than the
538 differences reported by Rodriguez et al. (2021) for the respective median travel times. To
539 summarize, ~~On a final~~ we argue ~~state~~ that standard deviations of travel times are distinct
540 ~~among~~ ~~between~~ the isotopes, particularly when ~~considering~~ ~~moving to~~ larger variances in
541 hydraulic conductivities. Maximum relative differences amount to 20% between HDO and
542 HTO as well as HTO and $^{18}\text{OH}_2$ (C3.1 and C3.2). ~~Which~~ ~~this~~ implies that the dispersion will
543 ~~vary~~ ~~differ~~ by approximately 40%.

544
545 ~~Again, we find that the average travel times of the different tracers increase with smaller~~
546 ~~diffusion coefficients of the water isotopes. Deuterium has the smallest self diffusion~~
547 ~~coefficient, but in all cases the largest average travel time, due a longer trapping in low~~
548 ~~conductive bottlenecks. The related differences between average travel times of deuterium and~~
549 ~~^{18}O rise clearly with increasing variance of the hydraulic conductivity field up to values of a~~
550 ~~110 days for the length of 60 m, compared to 50 days for $L = 30$ m.~~

551
552 ~~However, the average travel times at a given variance grow for each tracer almost~~
553 ~~proportionally to the transport distance. This implies that differences in $mean(T)$ between the~~
554 ~~tracers will not average out but grow with increasing transport distance and thus increasing~~
555 ~~average travel time. To corroborate this statement, we re-simulated tracer migration through the~~
556 ~~conductivity field with the variance 5 while lowering the average K_s to 1×10^{-8} m/s (Fig. 7).~~
557 ~~The differences between the average travel time of deuterium and ^{18}O are in the order of 2 years~~
558 ~~for the long and 1 year for the shorter system.~~

hat formatiert: Hochgestellt

hat formatiert: Tiefgestellt

hat formatiert: Schriftart: Kursiv

hat formatiert: Hochgestellt

hat formatiert: Tiefgestellt

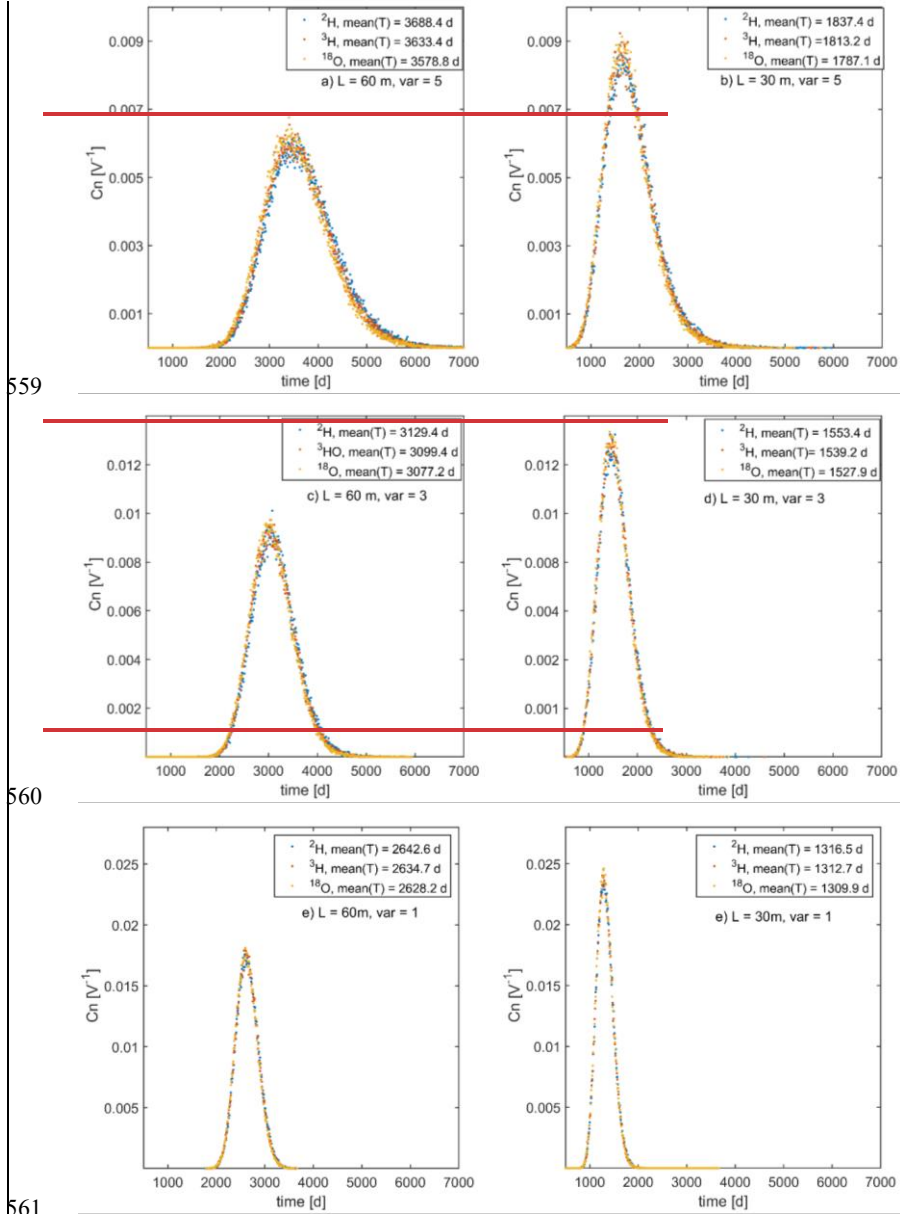
hat formatiert: Schriftart: Kursiv

hat formatiert: Schriftart: Kursiv

hat formatiert: Schriftart: Kursiv

hat formatiert: Hochgestellt

hat formatiert: Tiefgestellt



559

560

561

562

563

564

565

566

Figure 6: Normalized breakthrough and average travel time for scenario C for deuterium (^2H , blue dots), tritium (^3H , red dots) and ^{18}O (yellow dots) and corresponding average travel times $\text{mean}(T)$ after transport distances of 60 m (a, c, e) and 30 m (b, d, f). The variance of the hydraulic conductivity field decreases from top to bottom panels; the average K_s is 10^{-7} m/s .

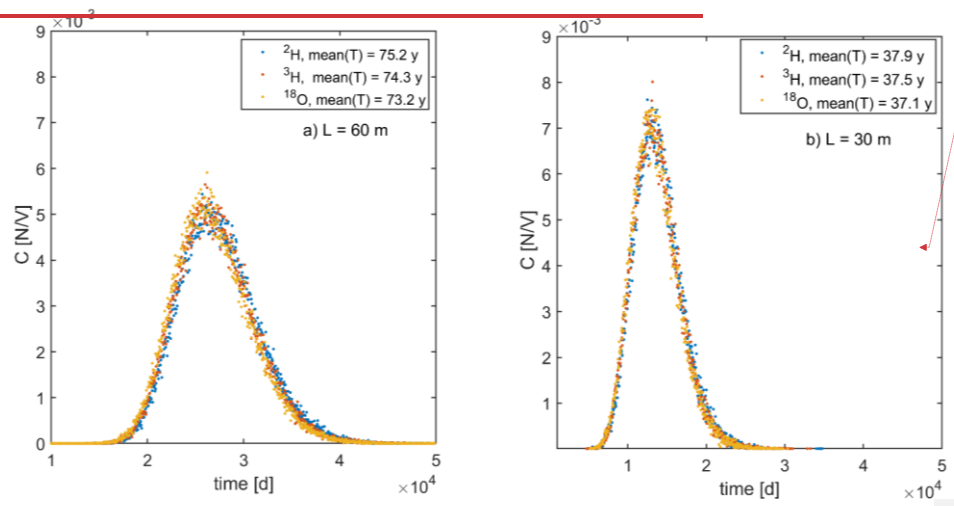
567 **4 DISCUSSION AND CONCLUSIONS**

568 Our study provides clear evidence that the sensitivity of average travel time distributions ~~TTDs~~
 569 to small changes in self-diffusion coefficients is – albeit partly relatively small – not a question
 570 of measurement error but a question of transport physics. Differences generally manifest
 571 generally as differences in higher quantiles and thus in the tailing behavior, as well as for the
 572 mean travel times and its standard deviations. Particularly, for the case of strongly
 573 heterogeneous, stochastic media and anomalous transport, we demonstrate that differences in
 574 average travel times of different water isotopes (~~H₂O~~HDO, ~~¹⁸O~~¹⁸OH²O, HDO) can deviate by
 575 as much as ~~two~~ 1.3 years, which corresponds ~~to~~ relative differences of 310% ~~of the average~~ and a
 576 maximum 50% ~~ge~~ travel time. We found the strongest relative differences of the order of ~~40~~ 50%
 577 for ~~a simple two-layered system~~ stochastic heterogeneous medium with a variance of 5 in the
 578 log hydraulic conductivity and a mean value of $K_s = 1 \times 10^{-6}$ m/s., ~~consisting of a mobile layer~~
 579 overlying a relatively immobile water storage compartment.

hat formatiert: Hochgestellt

hat formatiert: Hochgestellt

hat formatiert: Hochgestellt



Formatiert: Standard

580 Figure 7: Normalized breakthrough and average travel time for scenario C for deuterium (²H, blue dots), tritium
 581 (³H, red dots) and ¹⁸O (yellow dots) and corresponding average travel times *mean(T)* after transport distances of
 582 60 m (a) and 30 m (b). The variance of the hydraulic conductivity field is 5, while the average *K_s* is 10^{-8} .
 583

Formatiert: Listenabsatz

585 We found smaller differences of the order of 3 to 57% for strongly stochastically heterogeneous
 586 media. simple two layered media. Given their size, one could be inclined to erroneously interpret
 587 these differences as measurement errors. However, these differences are indeed physical and
 588 reflect tracers with smaller self-diffusion coefficients that eventually remain over longer times

589 in low conductive bottlenecks, which enlarges the tails and average travel times. Thus, these
590 effects do not average out, but persist when doubling the transport distances. ~~—even despite~~
591 ~~the total travel distances being 100 times larger than the short correlation length of the hydraulic~~
592 ~~conductivity field.~~

593
594 ~~We f~~Furthermore, we found that in the case of ~~the simple layered~~s systems and in heterogeneous
595 stochastic environments, the standard deviation and thus the dispersion of the travel times
596 ~~to grow distinctly grow~~ with declining self-diffusion coefficients, with a relative difference
597 ~~amount of up to values of 20%.~~ This is qualitatively the same behavior as what is known from
598 Taylor-Aris dispersion and confirms our related hypotheses.

599
600 Our findings are in line with the experiments of Elhanati et al. (2025) and corroborate that water
601 isotopes show similar behaviors to Br-. The molecular diffusion coefficient of bromide is
602 $2.01 \times 10^{-9} \text{ m}^2/\text{s}$, indeed close to that of HDO ($2.22 \times 10^{-9} \text{ m}^2/\text{s}$). Our study corroborates
603 furthermore the argument of Stewart et al. (2010, 2021), namely that averaged travel times
604 inferred from ^{18}O might in the case of two-layered mobile and immobile storage regions, or of
605 a strongly heterogeneous subsurface, be systematically shorter than those inferred from tritium.
606 The maximum differences we ~~found ranged between 90 d to 1.1~~ are 0.6 y, which correspond to
607 ~~a relative difference approximately 30%.~~ The latter corresponds to the difference Stewart et
608 al. (2010) reported for the Brugga catchment, which has an average travel time of order 3-6 y
609 for deep groundwater. Stewart et al. (2010) reported an even larger difference between
610 $\text{mean}(T_{18\text{OH}_2}) = 3.4 \text{ y}$ to $\text{mean}(T_{\text{T}_3\text{H}}) = 9.6 \text{ y}$ for the Pukemanga catchment. We cannot expect
611 to detect similarly large differences here, because we did not account for radioactive decay of
612 tritium (half-life of 12.32 years). Based on this decay one might detect contributions of rather
613 old water, that typically cannot be resolved based on differences in ^{18}O . ~~At this stage we come~~
614 ~~back~~return to the comprehensive demonstration of Wang et al. (2023), who found broadly
615 equivalent magnitudes of water ages inferred from ^3H and ^{18}O when using the SAS approach,
616 ~~while but~~ substantial differences ~~arose~~ when using a transfer function approach. ~~So e~~One could
617 ~~thus~~ be inclined to attribute at least ~~part~~some of the difference to the use of the transfer
618 function. However, in this context it is also important to note that Rodriguez et al. (2021) found
619 relative differences of approximately ~~0.23-%~~ in mean water ages in the Weiherbach using the
620 SAS approach and even larger differences as ~~corroborated as physical in this study.~~

hat formatiert: Hervorheben

622 ~~A comparison between the hydraulic retention times, inferred by dividing the storage volume~~
623 ~~by the flow, and average travel times, was in accord with the case of well-mixed advective-~~
624 ~~diffusive transport. The hydraulic retention times, however, systematically underestimated the~~
625 ~~average tracer travel times of the isotopic tracers, when transport was not well-mixed. This~~
626 ~~discrepancy can again be explained by diffusive trapping of tracers in rather immobile storage~~
627 ~~components: relatively long residence time cause the long tail in the breakthrough curve, which~~
628 ~~shifts the average travel time to the right.~~

629
630 We thus conclude that travel time distributions of isotopic tracers reflect the spectrum of fluid
631 velocities and diffusive/dispersive mixing between the flow lines connecting inputs and outputs
632 to the system. Travel time distributions of isotopic tracers might thus reflect the differences in
633 their self-diffusion coefficients, which are of order 10%, and in the case of non-Fickian
634 transport this eventually also affects substantially the mean travel time, it's variance, and in
635 particularly, travel times larger than the 80% quantile.

636
637 **Author contributions:** ~~EZ conducted most of the analysis and wrote the first draft of the paper.~~
638 ~~LP worked on the part explaining the role of water isotopes for inferring transit times, provided~~
639 ~~evidence on their self-diffusion coefficients and contributed to the writing. DE worked on the~~
640 ~~design of scenario A. BB contributed to the overall concept, theory and writing, particularly~~
641 ~~parts related to non-Fickian transport, and critically oversaw the study.~~Erwin Zehe conducted
642 ~~most of the analysis and wrote the first draft of the paper. Laurent Pfister worked on the part~~
643 ~~explaining the role of water isotopes for inferring transit times, provided evidence on their self-~~
644 ~~diffusion coefficients and contributed to the writing. Brian Berkowitz contributed to the overall~~
645 ~~concept, theory and writing, particularly parts related to non-Fickian transport, and critically~~
646 ~~oversaw/looked the study.~~

647
648 **Competing interests.** At least one of the (co-)authors is a member of the editorial board of
649 Hydrology and Earth System Sciences.

650
651 **Acknowledgements.** B.B. gratefully acknowledges the support of a research grant from the
652 Israel Science Foundation (Grant No. 1008/20); B.B. holds the Sam Zuckerberg Professorial
653 Chair in Hydrology. E.Z., B.B., and L.P. gratefully acknowledge the support of the ViTamins
654 project, funded by the Volkswagen Foundation (Grant No. 9B 192/-1), and of the LUNAQUA
655 project (Grant C21/SR/16167289), funded through the National Research Fund of
656 Luxembourg. The authors acknowledge support by Deutsche Forschungsgemeinschaft and the
657 Open Access Publishing Fund of Karlsruhe Institute of Technology (KIT). The service charges

658 for this open access publication have been covered by a Research Centre of the Helmholtz
659 Association.

660

661 5 REFERENCES

662

663 Barnes, C. and Bonell, M.: Application of unit hydrograph techniques to solute transport in
664 catchments, Hydrol. Process., 10, 793–802, 1996.

665 Bear, J., Dynamics of Fluids in Porous Media, Elsevier, 764 pp., 1972.

666 Benettin, P., Rinaldo, A., and Botter, G.: Tracking residence times in hydrological systems:
667 forward and backward formulations, Hydrological Processes, 29, 5203-5213,
668 10.1002/hyp.10513, 2015.

669 Benettin, P., Volkman, T. H. M., von Freyberg, J., Frentress, J., Penna, D., Dawson, T. E., and
670 Kirchner, J.: Effects of climatic seasonality on the isotopic composition of evaporating soil
671 waters, Hydrology And Earth System Sciences, 22, 2881-2890, 10.5194/hess-22-2881-2018,
672 2018.

673 Berkowitz, B. & Scher, H., On characterization of anomalous dispersion in porous and fractured
674 media, *Water Resour. Res.*, 31(6), 1461–1466, <https://doi.org/10.1029/95WR00483>, 1995.

675 Berkowitz, B., Cortis, A., Dentz, M. & Scher, H., Modeling non-Fickian transport in
676 geological formations as a continuous time random walk, *Reviews of Geophysics*, 44, RG2003,
677 <https://doi.org/10.1029/2005RG000178>, 2006.

678 Berkowitz, B., and Zehe, E.: Surface water and groundwater: unifying conceptualization and
679 quantification of the two "water worlds", Hydrology and Earth System Sciences, 24, 1831-
680 1858, 10.5194/hess-24-1831-2020, 2020.

681 Blöschl, G., and Zehe, E.: Invited commentary - On hydrological predictability, Hydrological
682 Processes, 19, 3923-3929, 2005.

683 Bolin, B. and Rodhe, H.: A note on the concepts of age distribution and transit time in natural
684 reservoirs, Tellus, 25, 58–62, 1973.

685 CELIA, M. A., BOULOUTAS, E. T., and ZARBA, R. L.: A General Mass-Conservative
686 Numerical-Solution For The Unsaturated Flow Equation, Water Resources Research, 26, 1483-
687 1496, 1990.

688 Dentz, M., Kirchner, J. W., Zehe, E., and Berkowitz, B.: The Role of Anomalous Transport in
689 Long-Term, Stream Water Chemistry Variability, Geophysical Research Letters, 50,
690 10.1029/2023gl104207, 2023.

691 Devel, L: Measurement of self diffusion in pure water H₂O-D₂O mixtures and solutions of
692 electrolytes. Acta Chem, Scand. 16, Vol. 9, 2177 -2188, 1962.

693 Edery, Y., Guadagnini, A., Scher, H., and Berkowitz, B.: Origins of anomalous transport in
694 heterogeneous media: Structural and dynamic controls, Water Resources Research, 50, 1490-
695 1505, 10.1002/2013wr015111, 2014.

696 Edery, Y., Dror, I., Scher, H., and Berkowitz, B.: Anomalous reactive transport in porous
697 media: Experiments and modeling, Physical Review E, 91, 10.1103/PhysRevE.91.052130,
698 2015.

699 Einstein, A.: Über die von der molekularkinetischen Theorie der Wärme geforderte Bewegung
700 von in ruhenden Flüssigkeiten suspendierten Teilchen. Annalen der Physik, 17, 549-560, 1905.

701 Elhanati, D., Zehe, E., Dror, I., and Berkowitz, B.: Transport behavior displayed by water
702 isotopes and potential implications for assessment of catchment properties, Hydrol. Earth Syst.
703 Sci., 29, 6577–6587, <https://doi.org/10.5194/hess-29-6577-2025>, 2025.

hat formatiert: Englisch (Vereinigte Staaten)

hat formatiert: Englisch (Vereinigte Staaten)

hat formatiert: Englisch (Vereinigte Staaten)

Feldfunktion geändert

Feldfunktion geändert

Formatiert: EndNote Bibliography

hat formatiert: Schriftart: (Standard) Times New Roman, 12 Pt., Englisch (Vereinigte Staaten)

hat formatiert: Englisch (Vereinigte Staaten)

704 ~~Elhanati, D., Zehe, E., Dror, I., and Berkowitz, B.: Transport behavior displayed by water~~
705 ~~isotopes and potential implications for assessment of catchment properties, EGU sphere~~
706 ~~[preprint], <https://doi.org/10.5194/egusphere-2025-3365>, 2025.~~
707 ~~Eriksson, E.: The possible use of tritium for estimating groundwater storage, *Tellus*, **10**, 472–~~
708 ~~478, 1958.~~
709 Hrachowitz, M., Soulsby, C., Tetzlaff, D., Dawson, J. J. C., and Malcolm, I. A.: Regionalization
710 of transit time estimates in montane catchments by integrating landscape controls, *Water*
711 *Resources Research*, **45**, W05421
712 10.1029/2008wr007496, 2009.
713 Hrachowitz, M., Benettin, P., van Breukelen, B. M., Fovet, O., Howden, N. J. K., Ruiz, L., van
714 der Velde, Y., and Wade, A. J.: Transit times the link between hydrology and water quality at
715 the catchment scale, *Wiley Interdisciplinary Reviews-Water*, **3**, 629-657, 10.1002/wat2.1155,
716 2016.
717 Jury, W. A., Simulation of solute transport using a transfer function model, *Water Resour.*
718 *Res.*, **18**(2), 363–368, 1982.
719 Klaus, J., Zehe, E., Elsner, M., Kull, C., and McDonnell, J. J.: Macropore flow of old water
720 revisited: experimental insights from a tile-drained hillslope, *Hydrology And Earth System*
721 *Sciences*, **17**, 103-118, 10.5194/hess-17-103-2013, 2013.
722 Klaus, J., Zehe, E., Elsner, M., Palm, J., Schneider, D., Schroder, B., Steinbeiss, S., van Schaik,
723 L., and West, S.: Controls of event-based pesticide leaching in natural soils: A systematic study
724 based on replicated field scale irrigation experiments, *Journal Of Hydrology*, **512**, 528-539,
725 10.1016/j.jhydro1.2014.03.020, 2014.
726 Kirchner, J., Feng, X. & Neal, C. Fractal stream chemistry and its implications for contaminant
727 transport in catchments. *Nature* **403**, 524–527 (2000). <https://doi.org/10.1038/35000537>
728 Levy, M., and Berkowitz, B.: Measurement and analysis of non-Fickian dispersion in
729 heterogeneous porous media, *Journal Of Contaminant Hydrology*, **64**, 203-226, 2003.
730 McGlynn, B., McDonnell, J., Stewart, M., and Seibert, J.: On the relationships between
731 catchment scale and streamwater mean residence time, *Hydrological Processes*, **17**, 175-181,
732 2003.
733 McGlynn, B. L., McDonnell, J. J., and Brammer, D. D.: A review of the evolving perceptual
734 model of hillslope flowpaths at the Maimai catchments, New Zealand, *Journal of Hydrology*,
735 **257**, 1-26, 2002.
736 ~~McGuire, K. J. and McDonnell, J. J.: A review and evaluation of catchment transit time~~
737 ~~modeling, *J. Hydrol.*, **330**, 543–563, 2006;~~
738 Rodriguez, N. B., McGuire, K. J., and Klaus, J.: Time-Varying Storage-Water Age
739 Relationships in a Catchment With a Mediterranean Climate, *Water Resources Research*, **54**,
740 3988-4008, 10.1029/2017wr021964, 2018.
741 Rodriguez, N. B., Pfister, L., Zehe, E., and Klaus, J.: A comparison of catchment travel times
742 and storage deduced from deuterium and tritium tracers using StorAge Selection functions,
743 *Hydrology and Earth System Sciences*, **25**, 401-428, 10.5194/hess-25-401-2021, 2021.
744 Sternagel, A., Loritz, R., Klaus, J., Berkowitz, B., and Zehe, E.: Simulation of reactive solute
745 transport in the critical zone: a Lagrangian model for transient flow and preferential transport,
746 *Hydrology and Earth System Sciences*, **25**, 1483-1508, 10.5194/hess-25-1483-2021, 2021.
747 Simmons, C. S., A stochastic-convective transport representation of dispersion in one-
748 dimensional porous media systems, *Water Resour. Res.*, **18**(4), 1193–1214, 1982.
749 Stewart, M. K., Morgenstern, U., and McDonnell, J. J.: Truncation of stream residence time:
750 how the use of stable isotopes has skewed our concept of streamwater age and origin,
751 *Hydrological Processes*, **24**, 1646-1659, 10.1002/hyp.7576, 2010.
752 Stewart, M. K., Morgenstern, U., and Cartwright, I.: Comment on "A comparison of catchment
753 travel times and storage deduced from deuterium and tritium tracers using StorAge Selection

hat formatiert: Englisch (Vereinigte Staaten)

hat formatiert: Englisch (Vereinigte Staaten)

754 functions" by Rodriguez et al. (2021), Hydrology and Earth System Sciences, 25, 6333-6338,
755 10.5194/hess-25-6333-2021, 2021.
756 Türk, H., Stumpp, C., Hrachowitz, M., Strauss, P., Blöschl, G., and Stockinger, M.: Catchment
757 transit time sensitivity to the type of SAS function for unsaturated zone and groundwater,
758 EGU sphere [preprint], <https://doi.org/10.5194/egusphere-2025-2597>, 2025.
759 Weiler, M., McGlynn, B. L., McGuire, K. J., and McDonnell, J. J.: How does rainfall become
760 runoff? A combined tracer and runoff transfer function approach, Water Resources Research,
761 39, 1315
762 10.1029/2003wr002331, 2003.
763 Wang, J. H, Robinson, Ch. V, Edelman, I. S.: Measurement of the Self-diffusion of Liquid
764 Water with, H3 and O18 as Tracers. Contribution from the Department of Chemistry of Yale
765 University, Department of Neurosurgery of New England Center Hospital, and Biophysical
766 Laboratory of Harvard Medical .School, 1952.
767 [Wang, S., Hrachowitz, M., Schoups, G., and Stumpp, C. Stable water isotopes and tritium
768 tracers tell the same tale: no evidence for underestimation of catchment transit times inferred
769 by stable isotopes in StorAge Selection \(SAS\)-function models. Hydrology and Earth System
770 Sciences. 27\(16\), 3083-3114, 2023.](#)
771
772 Wienhöfer, J., Germer, K., Lindenmaier, F., Färber, A., and Zehe, E.: Applied tracers for the
773 observation of subsurface stormflow on the hillslope scale, Hydrology and Earth System
774 Sciences, 13, 2009.
775 Zehe, E., Loritz, R., Edery, Y., and Berkowitz, B.: Preferential pathways for fluid and solutes
776 in heterogeneous groundwater systems: self-organization, entropy, work, Hydrology and Earth
777 System Sciences, 25, 5337-5353, 10.5194/hess-25-5337-2021, 2021.
778
779

hat formatiert: Englisch (Vereinigte Staaten)

hat formatiert: Englisch (Vereinigte Staaten)